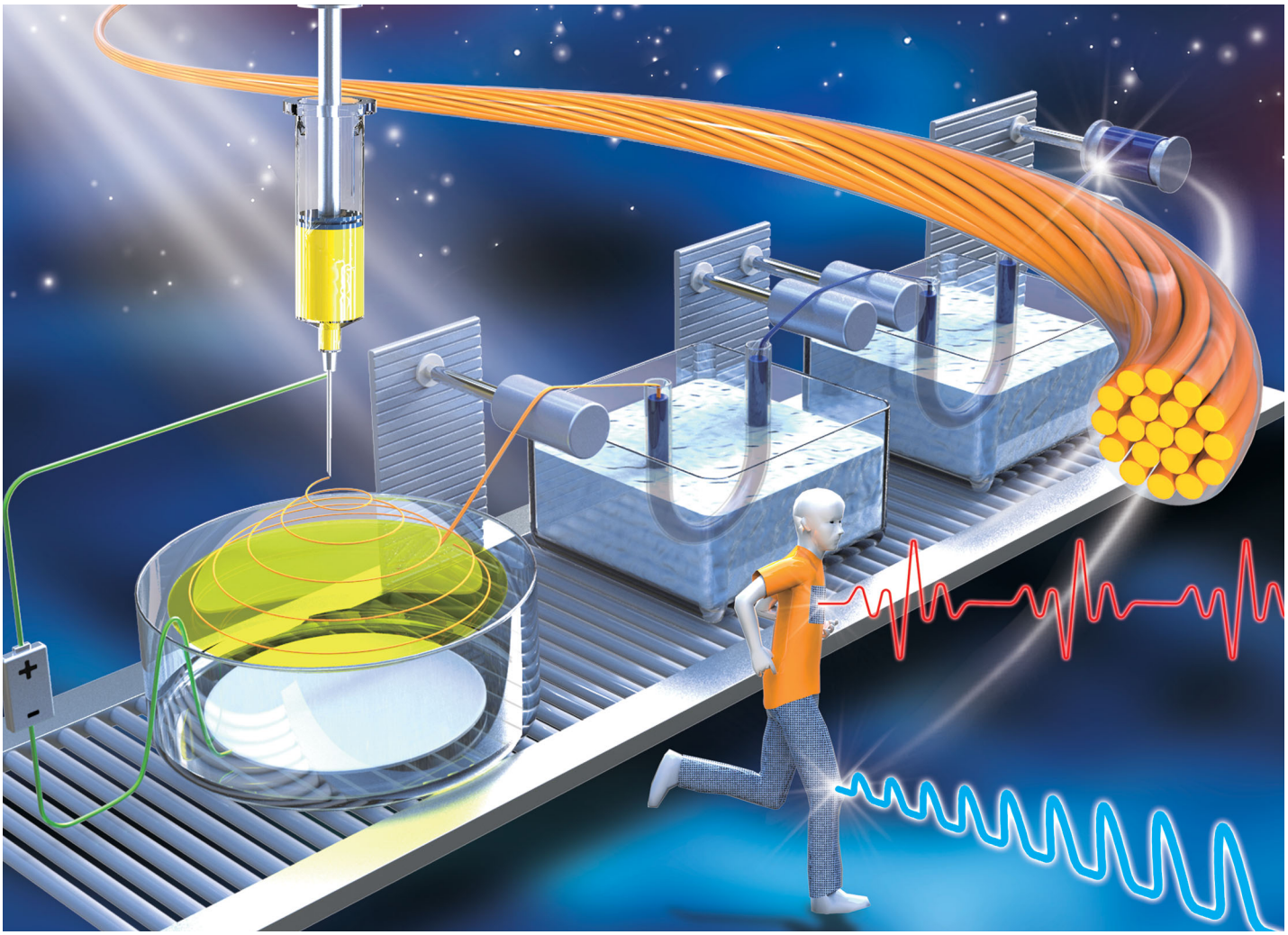

Showcasing research from The Key Laboratory of Material Processing and Mold of Ministry of Education, Zhengzhou University and Integrated Composites Lab, University of Tennessee

Continuously prepared highly conductive and stretchable SWNT/MWNT synergistically composited electrospun thermoplastic polyurethane yarns for wearable sensing

A one-step and continuous fabrication process is reported to fabricate composite electrospun fiber yarns with high conductivity and stretchability. These yarns can be easily integrated into strain sensors, exhibiting high stretchability with large workable strain range and good cyclic stability.

As featured in:

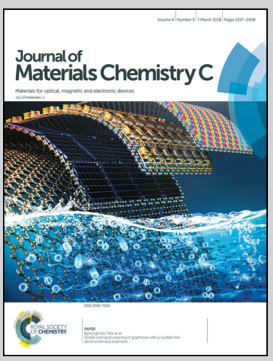

See Guoqiang Zheng, Xianhu Liu, Zhanhu Guo *et al.*, *J. Mater. Chem. C*, 2018, **6**, 2258.

ROYAL SOCIETY OF CHEMISTRY

rsc.li/materials-c

Registered charity number: 207890

Journal of Materials Chemistry C

PAPER

View Article Online
View Journal | View Issue

Cite this: J. Mater. Chem. C, 2018, 6, 2258

Continuously prepared highly conductive and stretchable SWNT/MWNT synergistically composited electrospun thermoplastic polyurethane yarns for wearable sensing†

Yahong Li,[a] Bing Zhou,[a] Guoqiang Zheng,*[a] Xianhu Liu,*[a] Tingxi Li,[b] Chao Yan,[c] Chuanbing Cheng,[d] Kun Dai,[a] Chuntai Liu,[a] Changyu Shen[a] and Zhanhu Guo*[d]

Highly conductive and stretchable yarns have attracted increasing attention due to their potential applications in wearable electronics. The integration of conductive yarns with large stretching capability renders the composite yarns with new intriguing functions, such as monitoring human body motion and health. However, simultaneously endowing the yarns with high conductivity and stretchability using an easily scalable approach is still a challenge. Here, highly conductive and stretchable yarns based on electrospun thermoplastic polyurethane (TPU) fiber yarns successively decorated with multi-walled carbon nanotubes (MWNTs) and single-walled carbon nanotubes (SWNTs) were prepared by a combined electrospinning, ultrasonication adsorbing, and bobbin winder technique. The improved thermal stability of the SWNT/MWNT/TPU yarn (SMTY) indicated strong interfacial interactions between the CNTs and electrospun TPU fibers. The synergism between the successively decorated SWNTs and MWNTs significantly enhanced the conductivity of the TPU yarns (up to 13 S cm^{-1}). The as-fabricated yarns can be easily integrated into strain sensors and exhibit high stretchability with large workable strain range (100%) and good cyclic stability (2000 cycles). Moreover, such yarn can be attached to the human body or knitted into textiles to monitor joint motion, showing promising potential for wearable electronics, such as wearable strain sensors.

Received 31st October 2017,
Accepted 24th November 2017

DOI: 10.1039/c7tc04959e

rsc.li/materials-c

1 Introduction

Next generation wearable electronic devices put forward increasingly stringent demands, such as direct wearing, portability and small element size.[1,2] Highly conductive yarns are ideal candidates for wearable electronics due to their fiber-shaped, flexible, wearable, and conformable characters.[3,4] Their potential applications as wearable electronic devices have been demonstrated, such as in yarn-based sensors,[5–7] flexible circuits,[8] human motion monitors,[9] and self-powered electronic textiles.[10] Among the conductive materials, such as carbon nanotubes (CNTs),[11] carbon fibers[12] and graphene,[13] for the preparation of highly conductive yarns, one-dimensional flexible CNTs, with their high electrical conductivity and remarkable mechanical properties,[14,15] exhibit more prospects for fabricating highly conductive yarns.[16–18] Earlier studies have mainly focused on developing pure CNT yarns. Most reports adopt dry spinning from aligned CNT matrices or direct spinning from chemical vapor deposition (CVD) reactions to fabricate macroscopic CNT yarns.[19–21] Although the aforementioned methods can obtain CNT yarns with superior mechanical properties and high electrical conductivity, these fabrication processes are complex, high-cost, and restricted in length and scalable production. Furthermore, based on pure CNT yarns, their composite yarns have been fabricated by incorporating the pure CNT yarns with polymers.[22,23] However, for both the pure CNT yarns and their composite counterparts, their stretchability is generally limited for wearable electronics covering the curved and moving surfaces of human skin. To improve stretchability, CNTs are always randomly dispersed into polymer matrices to fabricate conductive CNT/polymer composite yarns through wet-spinning,[24] electrospinning,[25] as well as other methods.[9,26] In some cases, the as-prepared composite yarns show a certain extent of stretchability while the

[a] College of Materials Science and Engineering, The Key Laboratory of Material Processing and Mold of Ministry of Education, Zhengzhou University, Zhengzhou, P. R. China. E-mail: gqzheng@zzu.edu.cn, xianhu.liu@zzu.edu.cn
[b] College of Materials Science and Engineering, Shandong University of Science and Technology, Qingdao 266590, China
[c] School of Material Science and Engineering, Jiangsu University of Science and Technology, No. 2, Mengxi Rd, Zhenjiang, Jiangsu, China
[d] Integrated Composites Laboratory (ICL), Department of Chemical & Biomolecular Engineering, University of Tennessee, Knoxville, TN 37996, USA. E-mail: zguo10@utk.edu

† Electronic supplementary information (ESI) available. See DOI: 10.1039/c7tc04959e

conductivity of such composites is relatively low because of the wrapping of insulating polymers on the surface of the CNTs.[26,27] What is worse is that CNTs tend to aggregate in the polymer matrices and thus deteriorate the yarn's mechanical performances.[28] Therefore, directly incorporating random CNTs into polymer solution is not an effective way to fabricate highly conductive and stretchable yarns.

It still remains a great challenge to simultaneously endow the CNT/polymer composite yarns with high conductivity and stretchability and new methods to overcome the aforementioned obstacles have been reported. For example, MWNT-adsorbed short electrospun PA66 nanofiber bundles with improved strength, robust flexibility and excellent conductivity have been demonstrated, but they are limited in the bundle length (only 3 cm) and scalable fabrication.[29] Based on the CNT sheets and elastomeric resin, Suzuki *et al.* fabricated highly conductive and stretchable ribbon that was also limited in the length because of the size of the CNT sheets.[30] Jin *et al.* also fabricated stretchable electronic fabric with multilayer assembly of more than three composites. However, the stretchability of the fabric was only 30% even with such a complicated method.[4] Researchers have also adopted the repeated melt bending of elastic polymers with MWNTs to fabricate composite fibers, while the conductivity and stretchability of the fibers were also restricted by the high-temperature processing conditions.[31] Thus, to fabricate highly conductive and stretchable yarns with a simple, low-cost, continuous, and scalable approach is still a big challenge for next generation wearable electronics.

In this study, polymer composite SWNT/MWNT/thermoplastic polyurethane (TPU) yarns (SMTY) with highly conductive and stretchable properties were prepared by a combined electrospinning, ultrasonication adsorbing, and bobbin winder technique. The successive decoration of MWNTs and SWNTs on the electrospun fibers showed a synergistic effect to obtain high conductivity of the SMTY and strong CNT–polymer interaction. Their structures and the interaction were characterized by Raman spectroscopy, X-ray diffraction (XRD) measurements, Fourier transform infrared (FTIR) spectroscopy, and differential scanning calorimetry (DSC). The effects of the CNTs on the thermal properties, electrical conductivity, mechanical properties, and morphology of the SMTY were also systematically studied. The successive decoration of the MWNTs and SWNTs exhibited a synergistic effect to obtain improved thermal properties and higher conductivity, as well as enhanced mechanical properties of the electrospun TPU fiber yarn. To fabricate strain sensors, the SMTY was embedded into PDMS. The response behaviors of the SMTY strain sensors under different strains and rates were conducted separately. Repeatability tests were used to test the durability of the strain sensors. Furthermore, the strain sensors were also woven into textiles to monitor human body motion.

2 Experiment section

2.1 Materials

Thermoplastic polyurethane (TPU, Elastollan 1185A), known for its better elasticity as a typical elastomer, was chosen for electrospinning and obtained from BASF Co., Ltd. Both the carboxylic MWNTs and unmodified SWNTs were purchased from Chengdu Organic Chemicals Co., Ltd, Chinese Academy of Science. The carboxylic MWNTs possessed a mean diameter of 20–40 nm, length of 30 μm, carboxyl content of 1.23 wt%, and purity over 95%. The SWNTs had a mean diameter of 1–2 nm, length of 5–30 μm, and purity over 95%. Sodium dodecyl sulfate (SDS, chemically pure) was purchased from Sinopharm Chemical Reagent Co., Ltd. Both *N*,*N*-dimethylformamide (DMF, ≥99.5%, analytical reagent) and tetrahydrofuran (THF, ≥90%, analytical reagent) were provided by Tianjin Fuyu Fine Chemical Co., Ltd, China. Deionized water was obtained from Dongguanshi nabaichuan water treatment equipment Co., Ltd.

A solution of TPU (22 wt%) was prepared using a mixture of DMF and THF (1 : 1) as the solvent. The carboxylic MWNTs (0.1 wt%) were dispersed in the deionized water with the surfactant SDS (0.5 wt%) and the SWNTs (0.05 wt%) were dispersed in deionized water with SDS (0.6 wt%). Both CNT dispersions were subjected to ultrasonication for 1 h at 0 °C on a Scientz-IID Ultrasonic Homogenizer (Ningbo Scientz Biotechnology Co., China) with a nominal frequency of 20 kHz and power of 285 W.

2.2 Continuous preparation of composite yarns

The continuous preparation setups were mainly composed of electrospinning, ultrasonication, and bobbin winder devices (refer to Fig. 1a). The electrospinning apparatus consisted of three components: (1) a high voltage supplier (DW-N503-4ACCD, Tianjin Dongwen High Voltage Power Supply Plant); (2) a spinneret with a diameter of 0.5 mm; (3) a water bath grounded collector electrode. Electrospinning was carried out at an applied voltage of 15 kV over a distance of 15 cm from spinneret to collector. The water bath grounded collector electrode consisted of a round glass petri dish. A round metal plate was placed inside the bath and covered with deionized water to a depth of 5 mm. A thin copper wire was trailed over the edge of the bath to connect the metal plate to the ground electrode. The environmental temperature and relative humidity were 30 ± 5 °C and 45 ± 5%, respectively. The ultrasonication apparatus consisted of two ultrasonic bathes (40 kHz and 100 W, Shengyuan Instrument Co., Ltd, China) and two U-shape glass tubes. For comparison with SMTY, a TPU fiber yarn (TY), MWNT/TPU fiber yarn (MTY), and SWNT/TPU fiber yarn (STY) were also fabricated.

2.3 Characterizations

The Raman spectra were obtained using a Horbia Labram-010 with 632 nm laser excitation at 1 cm^{-1} resolution in the range from 80 to 4000 cm^{-1}. The X-ray diffraction (XRD) measurements were carried out using a Rigaku Ultima IV X-ray diffractometer, equipped with a Cu tube and a scintillation detector beam. The XRD scans were recorded from 5° to 80° for 2θ with a 0.02° step-width and 60 s counting time for each step. Thermogravimetric analysis (TGA) was performed under nitrogen atmosphere on a TGA/TA Q50 (TA Instruments Co., USA) from room temperature to 700 °C with a heating rate of 20 °C min^{-1}. The electrical

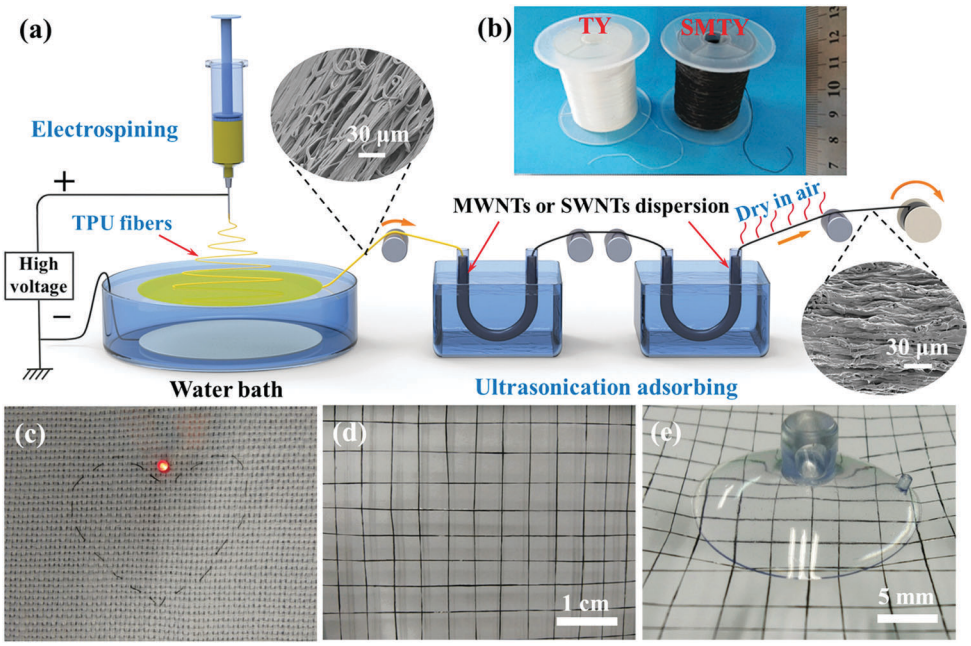

Fig. 1 A schematic illustration of the self-developed fabrication process for the composite fiber yarn (a); the optical images of the continuously rolled-up TY (left) and SMTY (right) (b); the optical image of the traditional cloth knitted with SMTY (c); the optical images of the electronic fabric composed of SMTY (d) and that under biaxial stretched condition (e).

resistance was measured by a high resistivity meter (TH2683, Changzhou Tonghui Electronics Co., Ltd) to evaluate the electrical conductivity. The distance between the two electrodes was 10 mm. To ensure accuracy, at least 8 specimens were tested for each condition. The samples were clamped with a pair of conductive copper tapes and silver paste was used to ensure good contact between the electrode and the sample. The current signals for the voltammetric measurement were recorded using a RST5200 electrochemical workstation (Suzhou Resitest Electronic Co., Ltd, China). For the mechanical property test, the yarn was first stabilized on a frame with a gauge length of 10 mm and then tested on a universal tensile testing machine (UTM2203, Sun Technology Stock Co., Ltd) equipped with a 100 N load cell at a crosshead rate of 10 mm min^{-1}. At least 8 specimens were tested to determine the final value of each condition. An Olympus BX51 optical microscope was used to determine the yarn diameter for the mechanical and electrical measurements. The surface morphology and cross section of the specimens were observed by scanning electron microscopy (JEOL JSM 7500F). Before observation, the specimens were sputtered with a thin layer of gold for better imaging. The Fourier transform infrared (FTIR) spectra of the yarns were acquired using a Nicolet iS50 spectrometer with the attenuated total reflection (ATR) mode. Differential scanning calorimetry (DSC) analysis was carried out using a DSC Q2000 (TA Instruments Co., USA). The samples were heated to 220 °C at a heating rate of 10 °C min^{-1} and held isothermally for 5 min to eliminate the effect of thermal history. Then the samples were cooled down to −50 °C and reheated to 220 °C at the same rate. All the tests were performed under the protection of N_2 gas at a flow rate of 20 mL min^{-1}.

2.4 Fabrication and characterization of the SMTY strain sensor

The SWNT/MWNT/TPU composite yarns were produced by combining electrospinning, ultrasonication adsorption, and bobbin winding in a continuous way. Fig. 1a illustrates the continuous process, which has benefit for realizing large-scale production. The self-designed fabrication process can be described as follows; the TPU random fibers were firstly electrospun and floated on the surface of the water. In a typical fabrication process, the initial non-woven web of fibers floating on the surface of the water were then drawn across the water and bundled into yarn with the aid of a revolving godet roller. The obtained continuous TPU fiber yarn was subsequently pulled into the U-shaped glass tubes that respectively contained the MWNT and SWNT dispersions and subjected to an ultrasonic bath for adsorbing the MWNTs and SWNTs. After drying in air with a hot wind dryer, the TPU fiber yarn successively decorated with MWNTs and SWNTs was finally collected by a cylindrical tube on the winding machine. The take-up roller's speed was set at 0.1 m min^{-1}. For comparison, the pristine TPU yarn (TY) was also continuously electrospun through water-bath collection but it was not subjected to the ultrasonication process.

To fabricate the SMTY strain sensor, the yarn was first cut into segments and both ends of the segment were coated with conductive silver paste to eliminate contact resistance. The whole specimen was stabilized on a frame and PDMS was coated to obtain good encapsulation. The PDMS base and curing agent (Sylgard 184, Dow Corning) were first mixed in a mass ratio of 10 : 1 to form liquid PDMS. Subsequently, the liquid PDMS was uniformly coated onto the whole specimen and then cured at 60 °C for 2 h to form the final strain sensor. The precision digital resistor and universal testing machine

were connected with a computer to monitor the strain sensing behaviors. The strain value (ε) is defined as the ratio of the length change (ΔL) to the initial length (L_0). The relative resistance change ($\Delta R/R_0$) is defined as the ratio of the resistance change (ΔR) to the resistance (R_0) at the initial state. The strain gauge factor (GF, defined as $(\Delta R/R_0)/\varepsilon$) is applied to evaluate the strain sensitivity of the strain sensor.

2.5 Motion monitoring experiment

To demonstrate the potential applications of SMTY strain sensors as wearable electronic devices, they were fixed on cloth tapes or knitted into textiles to monitor human motion. By virtue of the flexibility of the yarn, it can be readily cut into an appropriate length and assembled.

3 Results and discussion

3.1 Continuous preparation of the SWNT/MWNT/TPU yarns

Fig. 1b shows the continuously rolled-up TY and SMTY. SMTY can be readily knitted into traditional fabrics with arbitrary shape and constructed into a simple circuit to power a light-emitting diode (LED) (Fig. 1c). In addition, it can be assembled into a large area electronic fabric (Fig. 1d), in which each cross contact can form a sensor unit. Moreover, the fabric sensor array is stretchable (Fig. 1e) and can be applied on arbitrary curved and moving surfaces.

Raman spectroscopy was performed to analyze the structure of the SWNTs, MWNTs, TY and SMTY (Fig. 2a). For SWNTs, three typical peaks at 1324, 1591, and 2639 cm^{-1} are presented, corresponding to the D, G, and 2D bands, respectively, which are the signatures of the CNT structure. As is well known, the D band is related to the defects induced by disorder, whereas the G and 2D bands correspond to the in-plane vibration of the C–C bond.[32,33] For MWNTs, the characteristic peaks of CNTs are also evident.[34] For TY, the characteristic vibration bands of TPU can also be recognized: *i.e.*, the peak at 1447 cm^{-1} is due to the bending vibrations of $-CH_2$; the strong peak at 1614 cm^{-1} corresponds to the aromatic breathing mode symmetric stretch vibration of C=C; and the characteristic peak at 2926 cm^{-1} is attributed to the stretching vibrations of $-CH_2$.[35,36] In the spectrum of SMTY, the characteristic bands of the CNTs are easily identified. Compared with the spectra of the SWNTs and MWNTs, it is worth noting that several characteristic peaks of the CNTs have been up-shifted. For example, the D band peak is up-shifted from 1324 to 1328 cm^{-1}, and the G band increases from 1591 to 1594 cm^{-1}. What is more, one of the characteristic peaks of TPU is also up-shifted from 2926 to 2934 cm^{-1} by 8 cm^{-1} after the decoration of the SWNTs and MWNTs (seen in the inset in Fig. 2a). Moreover, the other TPU characteristic bands become less obvious or even disappear after the decoration of the MWNTs and SWNTs. All these observations evidence the existence of strong interface interaction between the SWNTs, MWNTs, and electrospun TPU fibers.

Fig. 2b displays the XRD spectra of the SWNTs, MWNTs, TY, and SMTY. The SWNTs are observed to exhibit a weak broad diffraction peak at around 26.4°, and a weaker diffraction peak at 44.5°, which can be attributed to the (002) and (100) planes of a graphitic structure. The diffraction peaks of the MWNTs are also observed at about 25.9° (002) and 43.3° (100), which are ascribed to the interlayer space in the radial direction and the in-plane graphitic structure of the CNT, respectively.[37] Moreover, pure TPU in TY displays a diffraction peak at about 20.4°, which is relevant to the existence of a short range regularly ordered structure of both hard and soft domains along with a disordered structure of the amorphous phase of the TPU matrix.[38,39] The characteristic peak of TPU can be easily identified in the XRD cure of SMTY, indicating that the crystal structure of the TPU matrix remains unchanged after the decoration of the CNTs. On the other hand, its intensity is attenuated after the decoration of the CNTs. This phenomenon may be resulting from the interfacial interaction between the TPU and CNTs, causing the decrease in the crystalline size of TPU.[39]

3.2 Thermal stability and electrical conductivity

For comparison with SMTY, SWNT/TPU fiber yarn (STY) and MWNT/TPU fiber yarn (MTY) were also fabricated. TGA was performed to evaluate the thermal stability and CNT content of these composite yarns. As shown in Fig. 3a, the TGA curves for STY, MTY, and SMTY shift towards higher temperatures compared with TY, indicating that the thermal stability of the

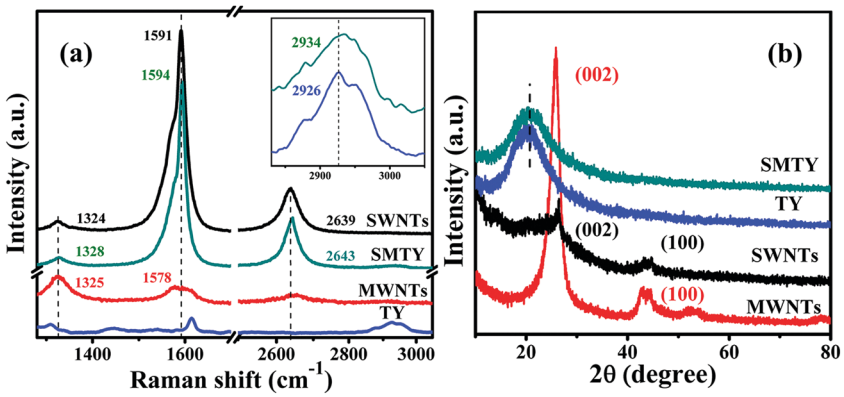

Fig. 2 The Raman spectra (a) and XRD spectra (b) of the SWNTs, MWNTs, TY and SMTY.

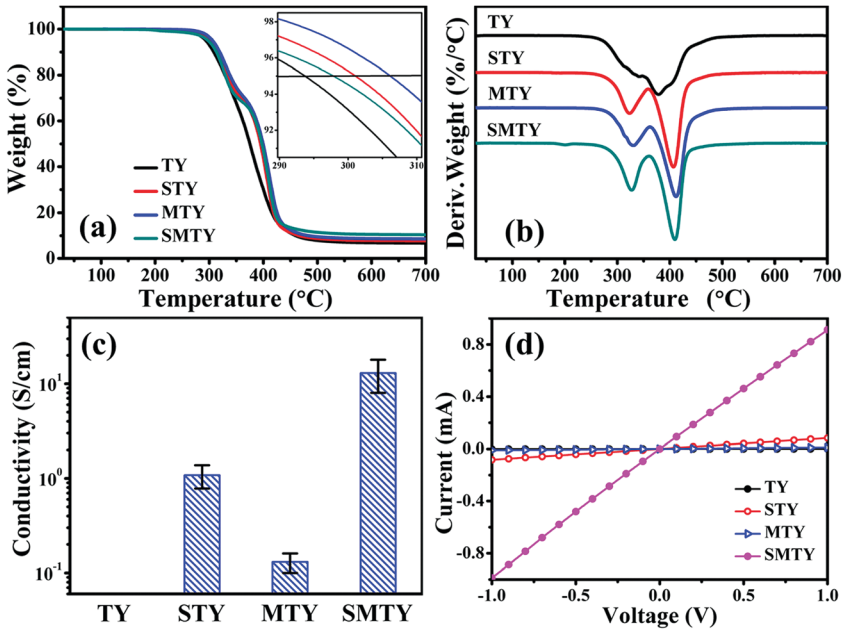

Fig. 3 The TGA curves (a) and DTG curves (b) of the yarns; the conductivity (c) and the *I*–*V* curves (d) of the yarns.

electrospun TPU fibers is improved after the decoration of CNTs. A two-step degradation process is obviously observed from the corresponding derivative thermogravimetric (DTG) curves in Fig. 3b. The first step is related to the cleavage of the urethane bonds of TPU and the second one is attributed to the decomposition of the soft segments of TPU.[34] Compared with TY, the T_{max} (the temperature at which the maximum DTG occurs) of the SMTY increases from 379 to around 410 °C, suggesting that the successive decoration of the SWNTs and MWNTs can bring a positive effect on the improvement of the thermal stability. The enhanced thermal stability may result from the perfect distribution of CNTs as well as strong interaction between the CNTs and electrospun TPU fibers. The CNT content of these yarns can be obtained from the TGA and listed in Table S1 (ESI†). The electrical conductive behaviors of these composite yarns are listed in Fig. 3c and d. The volume conductivity is calculated using the equation: $\sigma = L/RS$, where σ is the volume conductivity, L is the length of the yarn between the electrodes, R is the volume resistance, and S is the cross-section area of the yarn. As shown in Fig. 3c, TY is electrically insulative while the conductivity is significantly improved after the decoration of the MWNTs and SWNTs. Clearly, the conductivity of MTY reaches around 0.13 S cm^{-1} while STY is approximately 1.08 S cm^{-1}, the increased conductivity is due to the fact that SWNTs have a higher conductivity than MWNTs. More interestingly, after the successive decoration of the carboxylic MWNTs and SWNTs with a total content of 3.65 wt% (see Table S1, ESI†), the conductivity of SMTY significantly increases to 13 S cm^{-1}, which is unexpectedly 100 times as high as MTY and 12 times as high as STY. To our knowledge, this value is the highest among those fibrous composites with CNTs absorbed *via* ultrasonication.[29,40–43] Fig. 3d shows the typical *I*–*V* curves. It can also be seen that the *I*–*V* curve of the TY is a horizontal line, showing no evidence of electrical signals, while other samples display typical Ohmic behavior, indicating stable electrical properties.

The significantly improved conductivity must be attributed to the formation of a CNT conductive network on the TPU fibers. These electrospun TPU fibers possess a very high surface area and can provide a large position for lots of CNTs to attach. Furthermore, the higher conductivity of SMTY over other yarns indicates that a synergetic conductive network was constructed by the MWNTs and SWNTs. This synergetic conductive network can be understood from three points. Firstly, adsorbing the carboxylic MWNTs may improve the hydrophilic performance of the pristine TPU fiber yarn and promote the attaching of the SWNTs in aqueous medium;[44] secondly, SWNTs with large aspect ratios are mechanically flexible, this allows them to conform to the topological morphology of the fibers firstly adsorbed to the MWNTs; thirdly, SWNTs have been proven to have large van der Waals interactions with polymers.[45] In a word, a synergy conductive network has been constructed during the continuous fabrication process, producing highly conductive SMTY with lower CNT content. The perfect conductivity and Ohmic behavior of SMTY suggest that such yarn can act as an ideal electrode for further functional applications.

3.3 Mechanical properties

Fig. 4a shows the typical stress–strain curves of the yarns. The mechanical parameters can be obtained from the stress–strain curves, Fig. 4b. Clearly, compared with TY, the significantly improved tensile strength is observed with the incorporation of CNTs. For example, the tensile strength of SMTY has been increased by up to 250% compared with TY, by up to 80% compared with MTY, and by up to 30% compared with STY. The improvement can be ascribed to the following two aspects. (1) The CNTs adsorbed on the surface of the electrospun fiber

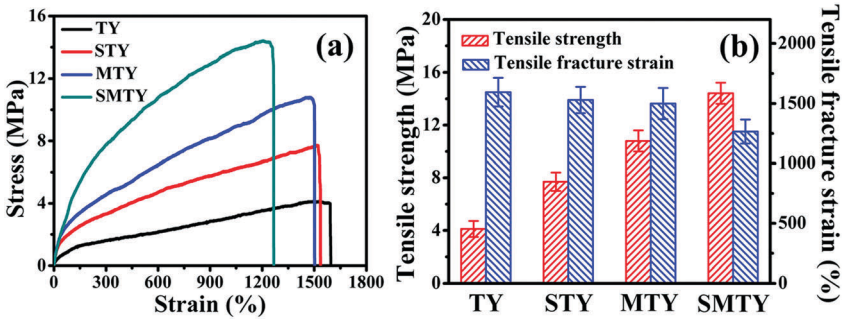

Fig. 4 The typical stress–strain curves (a) and specific mechanical properties (b) of the yarns.

will draw the fibers closer and decrease the slippage of the fibers by interconnecting them, resulting in a higher tensile strength, which has also been observed in the research of MWNT-adsorbed electrospun PA66 bundles;[29] (2) the CNTs will hit the fibers strongly and be anchored onto the fibers tightly, leading to strong interactions between the CNTs and fibers, which have been confirmed by the Raman spectra and FTIR spectra. More interestingly, although the fracture strain of the SMTY decreases slightly compared with TY, it still stays over 1200% (see Fig. 4b), indicating that SMTY remains ductile even when it is as large as possible and meets the deformation demand of wearable electronics.

3.4 Morphology

In order to better understand the electrical conductivity and mechanical properties of the SMTY, the surface morphologies of the yarns were observed by SEM. Fig. 5a–a″ show the typical SEM images of the TY, which is a ribbon composed of numerous electrospun TPU fibers (diameters of 1–2 μm) with high surface area. Generally, the electrospun TPU fibers are observed to have uniform diameters and smooth surfaces. Apart from some randomly arranged ones, most fibers align along the yarn's longitudinal axis. Moreover, there is spacious interspacing between the adjacent fibers which is helpful for the CNTs to

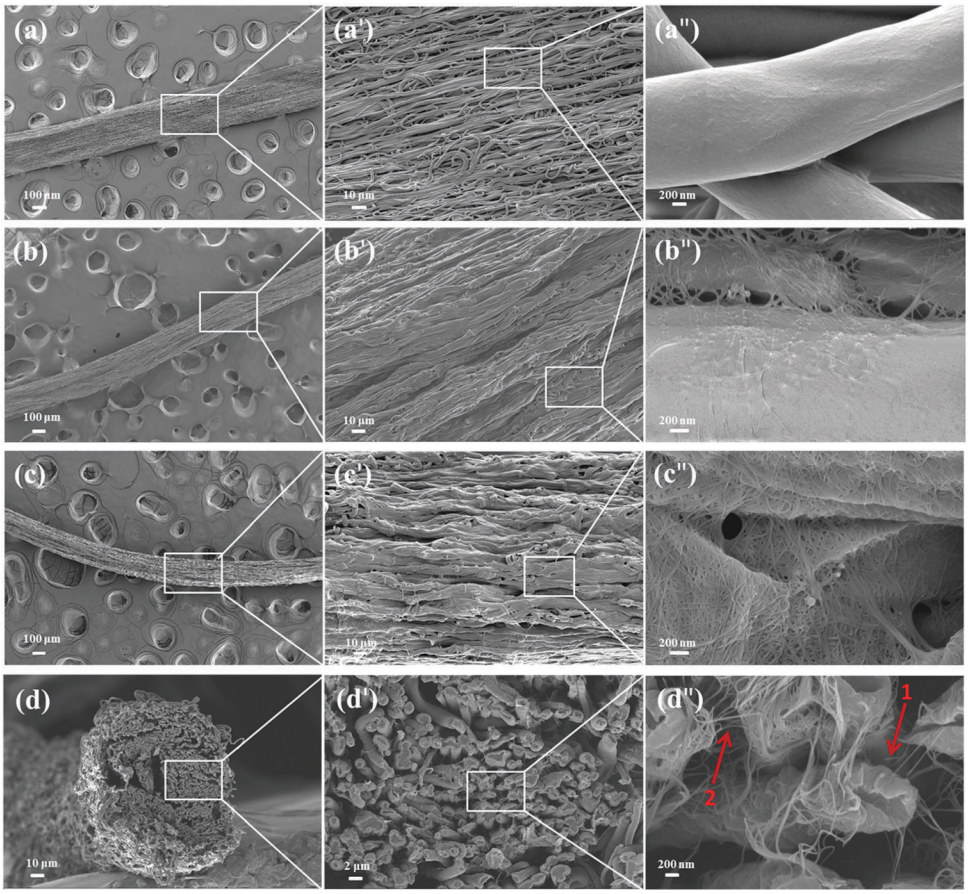

Fig. 5 The surface morphologies of TY (a–a″), MTY (b–b″) and SMTY (c–c″) and the cross section morphology of SMTY (d–d″) at different magnifications.

enter and for decoration. After the decoration of the MWNTs, the outline shape of the yarn changes from ribbon to cylinder (Fig. 5b) and the distance between the neighboring fibers obviously decreases, which can be confirmed by the high-magnification SEM pictures (see Fig. 5b′). The changed shape and the decreasing distance can be ascribed to the fact that ultrasonication can provide a physical shake to rearrange the stacking state of the fibers. Moreover, MWNTs have tightly adsorbed onto the surface of the fibers and act as bridges joining one fiber with other ones, while the fibers are not entirely covered by the MWNTs (see Fig. 5b″). After the successive decoration of the MWNTs and SWNTs, the yarn diameter has no obvious changes (Fig. 5c). Interestingly, the whole fibers are completely covered with MWNTs and SWNTs, and even the spaces between the fibers are densely covered by CNT films (see Fig. 5c″). Fig. 5d–d″ shows the cross sections of SMTY prepared by freeze cutting. The approximate circle shape of the cross section shown in Fig. 5d further confirms the rearrangement effect of ultrasonication, and many cross sections of the TPU fibers can be seen in Fig. 5d′, indicating that most electrospun fibers align along the longitudinal direction of the yarns. This is well consistent with Fig. 5a″. As shown in Fig. 5d″, the interior fibers in the yarn are entirely covered by a dense CNT layer, which can be confirmed by the wrinkled CNT layer surrounding the cross section of the fiber (see arrow 1). Moreover, the TPU fibers are also well joined by numerous CNTs (see arrow 2), demonstrating that the CNTs have entered the interior region of the yarn and formed a three-dimensional CNT network upon ultrasonication.

3.5 Interface interaction between the CNTs and TPU fibers

FTIR spectroscopy was further performed on TY and SMTY to analyze the interface interaction between the CNTs and TPU fibers. The main characteristic peaks of the samples are shown in Fig. 6a. For the pure TPU fibers, the peak at 3328 cm^{-1} is the characteristic N–H stretching band of urethanes, and the peak at 1727 cm^{-1} is assigned to the free carbonyl group in the urethane linkage (–H–N–COO–). Furthermore, the peak at 1529 cm^{-1} is associated with the combination of N–H bending and C–H stretching. In addition, the stretching C–O and C–O–C bands are present at 1130 and 1076 cm^{-1}, respectively. However, it can be found that several peaks for the TPU fibers have shifted after the decoration of the MWNTs and SWNTs. For example, the peak at 1130 cm^{-1} has shifted to 1124 cm^{-1} and the peak at 1076 cm^{-1} has shifted to 1059 cm^{-1}. These changes also suggest chemical interactions between the TPU macromolecular chain and the CNTs.[36] More importantly, a Scotch tape peeling test was conducted to evaluate the adhesion of the CNTs on SMTY. The result shows that CNTs cannot be easily wiped off from the SMTY (refer to Fig. S1, ESI†), indicating a strong interface interaction between the MWNTs, SWNTs and electrospun TPU fibers.

DSC experiments were also carried out to investigate the effect of the interaction on the thermal properties of TPU. As shown in Fig. 6b, the glass transition temperature (T_g) of TY is found to be −23.68 °C. After the decoration of the MWNTs and SWNTs, the T_g of SMTY increases to −22.08 °C. The enhanced T_g indicates that the TPU chains were constrained by the interface interaction between TPU and the CNTs.[46] This phenomenon is also consistent with the TG results shown in Fig. 3a.

3.6 Strain sensor characterization

Due to the high conductivity and large ductility, the SMTY was selected to assemble into wearable strain sensors. As shown in Fig. 7a, a SMTY strain sensor was fabricated by encapsulating single SMTY in PDMS. Fig. 7b shows that the encapsulated SMTY can be steadily stretched to a strain of 100%, indicating excellent stretchability. More importantly, the encapsulated SMTY exhibits better resistance recoverability even after the stretch/release cycle of ε = 100% (see Fig. 7c). The resistivity is calculated by using the equation: $\rho = RS/L$, where ρ is the resistivity, R is the volume resistance, S is the cross-section area of the yarn, and L is the length of the yarn between the electrodes. Under the cyclic loading of 100% strain, the resistivity changes from 0.07 to 0.08 Ω cm. The resistivity cannot return to the initial state completely, which is related to the non-recoverable change in the molecular and supermolecular chains of TPU.[36] The change of resistivity is not so obvious, which also indicates the stability of the strain sensing. In contrast, as for SMTY, even after the cycle of ε = 50%, its resistance is hardly recovered with the change of resistivity from 0.07 to 0.09 Ω cm. Thus, PDMS is employed in this work to endow the strain sensor with

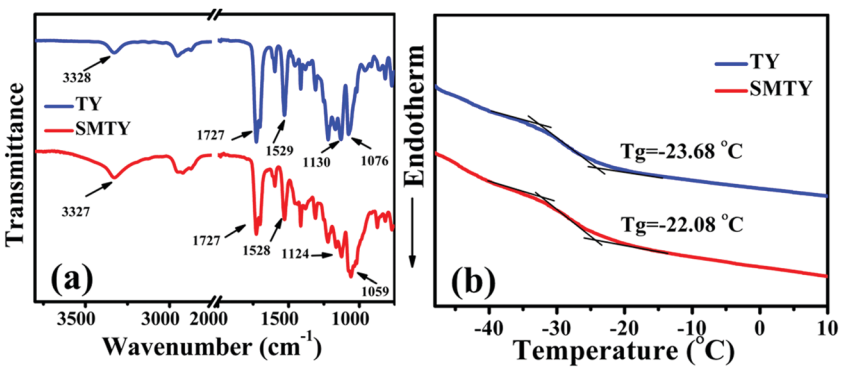

Fig. 6 The FTIR spectra (a) and the DSC curve (b) of the TY and SMTY.

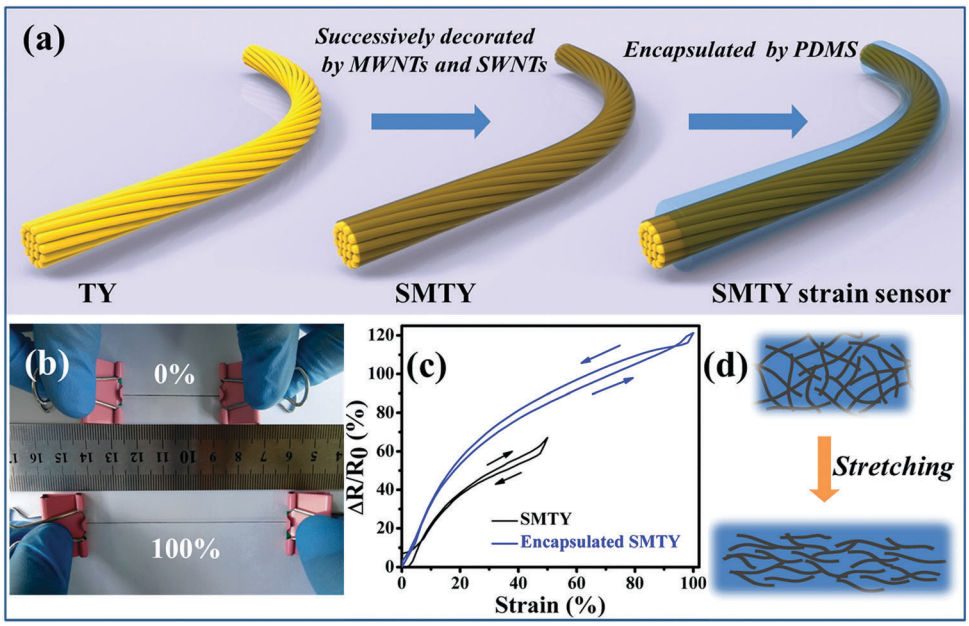

Fig. 7 The fabrication of the SMTY strain sensor (a); the optical image of the SMTY strain sensor before and after stretching of ε = 100% (b); the response behaviors of the SMTY and encapsulated SMTY under the stretch/release cycles (c); a schematic illustration of the strain sensing mechanism (d).

better stability. To better understand the stable mechanism of the SMTY strain sensor, its cross section was observed by SEM (Fig. S2, ESI†). The liquid PDMS was completely penetrated into the yarn and it filled the interspace between the CNT-decorated fibers, forming a firm composite structure of the SMTY and PDMS. Particularly, the CNT network surrounding the fibers is well fixed by the immersed PDMS (Fig. S2c and d, ESI†), thus preventing the conductivity network from excessive damage upon the large stretching. Moreover, the stretchable PDMS also promotes good recoverability of the SMTY strain sensor. The stretchable mechanism of the SMTY strain sensor can be illustrated in Fig. 7d. When the SMTY strain sensor is subjected to stretching, the overlapping area of the CNTs decreases resulting in the increased electrical resistance; after releasing, the electrical resistance returns with the recovery of the elastic TPU fiber and PDMS.

As shown in Fig. 8a, a resistance variation characteristic of the SMTY strain sensor is observed with the strain varying from 0 to 200%. The strain rate is set to be 10 mm min^{-1}. The sensor resistance change exhibits a positive correlation with the increasing strain. The curve can be divided into at least two linear regions with different slopes before the strain of 100%. In the strain range from 0 to 20% (see the inset of Fig. 8a), the average calculated gauge factor (GF) is about 1.67. In the strain range of 20–100%, the average GF is about 1.24. The difference of GF originates from the fact that the damage extent of the conductive network is different with increasing the strain.[36,47,48] As shown in Fig. 5d″, the TPU fibers are well joined by numerous CNTs. When a small strain is exerted, the CNT network among the fibers firstly breaks down and mainly leads to increase of the resistance. With increasing the strain, the breakdown of the CNT networks on the surface of the fibers and the increase of the distance both lead to an increase of resistance. Fig. 8b shows the sensory response under different cyclic strains with the same strain rate. The relative resistance change increases as the strain increases, which is in good accordance with the result shown in Fig. 8a. Obviously, the SMTY strain sensor can be employed to detect large strain (20–100%) as well as smaller strain (see Fig. 8c). It is worth noting, such larger workable strain (*i.e.*, 100%) of our SMTY strain sensor gains an advantage over other yarn-based strain sensors (*e.g.*, less than 30%).[4,49,50]

The larger workable strain suggests that such a SMTY strain sensor has potential applications as wearable electronics. For example, since human skin has an average elongation from 3% to 55%,[1] it can be used for monitoring human motion (see Fig. 9). Fig. 8d shows the relative resistance change of the SMTY strain sensor with a strain of 50% at different strain rates. This chart reveals that the applied rate range (5–25 mm min^{-1}) affects the relative resistance change weakly, which is of great importance to obtain a reliable response. To evaluate the durability of this sensor, Fig. 8e shows the performance of the sensor under a cyclic loading of 50% strain at a rate of 10 mm min^{-1} for 2000 cycles. In the initial strain testing, there is a slight downward trend in the relative resistance change. After some of the initial stretching/relaxing cycles, the sensor exhibited stability during the cyclical loading and unloading processes. This repeatability test demonstrates that such a SMTY strain sensor has good durability. To study the humidity and temperature effect on the stability of the SMTY strain sensor, the humidity and temperature sensing behaviors are shown in Fig. S3 (ESI†). As shown in the curve of humidity sensing, the relative resistance change increases a little with the relative humidity changing from 11% to 75%, indicating the stability of the strain sensor in different humidities. This may

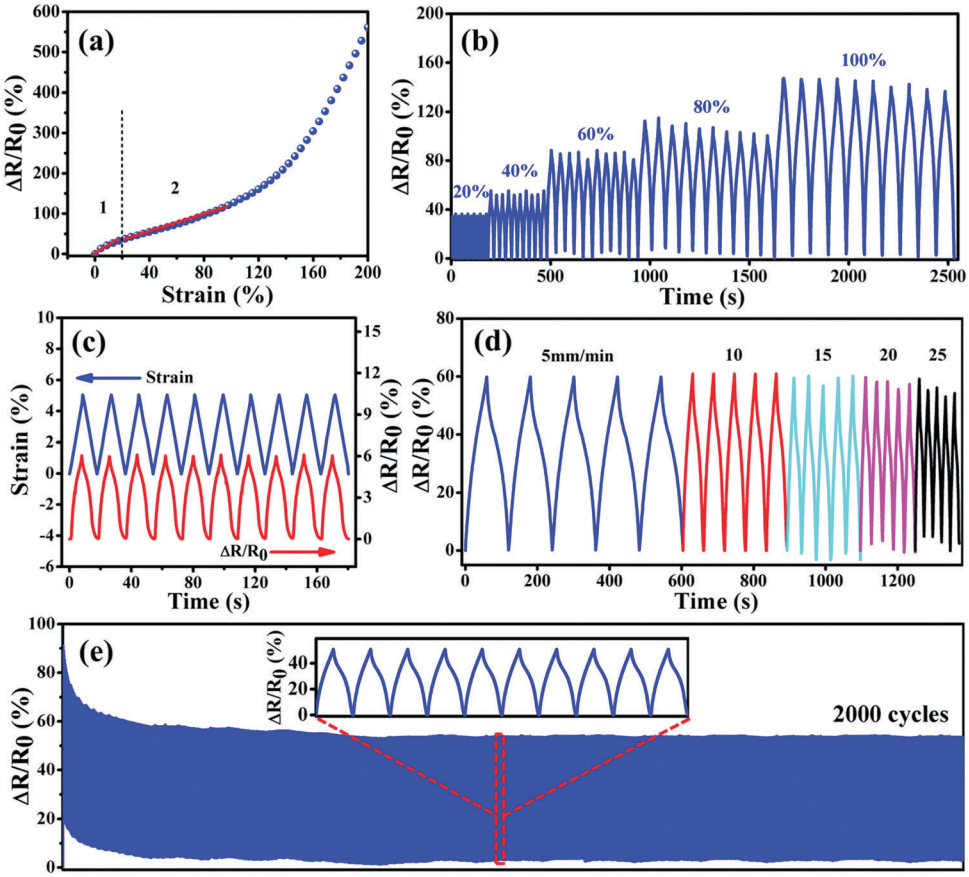

Fig. 8 The basic characteristics of the SMTY strain sensors. The relative resistance change *versus* the applied strain of up to 200% (a); the relative resistance change with various cyclic strains at a strain rate of 10 mm min^{-1} (b); the relative resistance change under small cyclic strain of 3% (c); the relative resistance variation with a strain of 50% at different strain rates (d); the performance of the SMTY sensor under cyclic tensile loading for 2000 cycles (e).

be ascribed to the protection of PDMS, which prevents the conductive network from being excessively damaged. From the curve of temperature sensing, the relative resistance change decreases slowly with increasing the temperature from 10 to 80 °C, indicating a negative temperature coefficient effect.[29] However, the relative resistance change is lower than 0.02 before 40 °C (close to the limit of room temperature). For the wearable strain sensor, this resistance change may be weak compared with the strain sensor. Thus, to some extent, the SMTY strain sensor shows the property of humidity resistance and temperature resistance for wearable device application.

3.7 Motion monitoring experiment

The yarn-based strain sensors have great potential in serving as wearable electronic devices due to their weavability into textiles.[51] In order to demonstrate the potential applications of the SMTY strain sensors as wearable devices, they are assembled into various devices to monitor different human motions. By virtue of the flexibility and widely workable strain range, a large range of motions of the human body, such as the motions of joints, can be recognized by this sensor. Being fixed onto a neck with an elastic bandage, it can monitor the motion of the neck joint. As shown in Fig. 9a, when the man begins to look down, the relative resistance change increases and reaches a maximum value. With the relaxation of the neck, the relative resistance change decreases and returns to the original position. The sensory response to the cyclic motion of the neck also indicates that the SMTY strain sensor is stable during the monitoring process. A similar measurement is conducted on a wrist with continuous bending, and the strain sensor also exhibits good performance (Fig. 9b). Based on the flexible fiber shape, the SMTY stain sensor can be readily cut into an appropriate length and knitted into textiles without any other assistance. It can be seen from Fig. 9c that such a sensor can be easily knitted into fabric cloth as long as needed. The prompt response and regular relative resistance change prove that it can be employed to monitor a large range of knee motions. Apart from being knitted into cloth, it can be fixed on the surface of cloth with the help of PDMS. As shown in Fig. 9d, the elbow motion can also be well recognized by the sensor. To monitor finger bending, the SMTY strain sensor is fixed along the finger joint line on the surface of a rubber glove. The bending of the metacarpophalangeal (MP) joint, proximal interphalangeal (PIP) joint, and distal interphalangeal (DIP) of one finger are separately detected. During each test, the finger firstly stays extended and then bends to a limited angle.

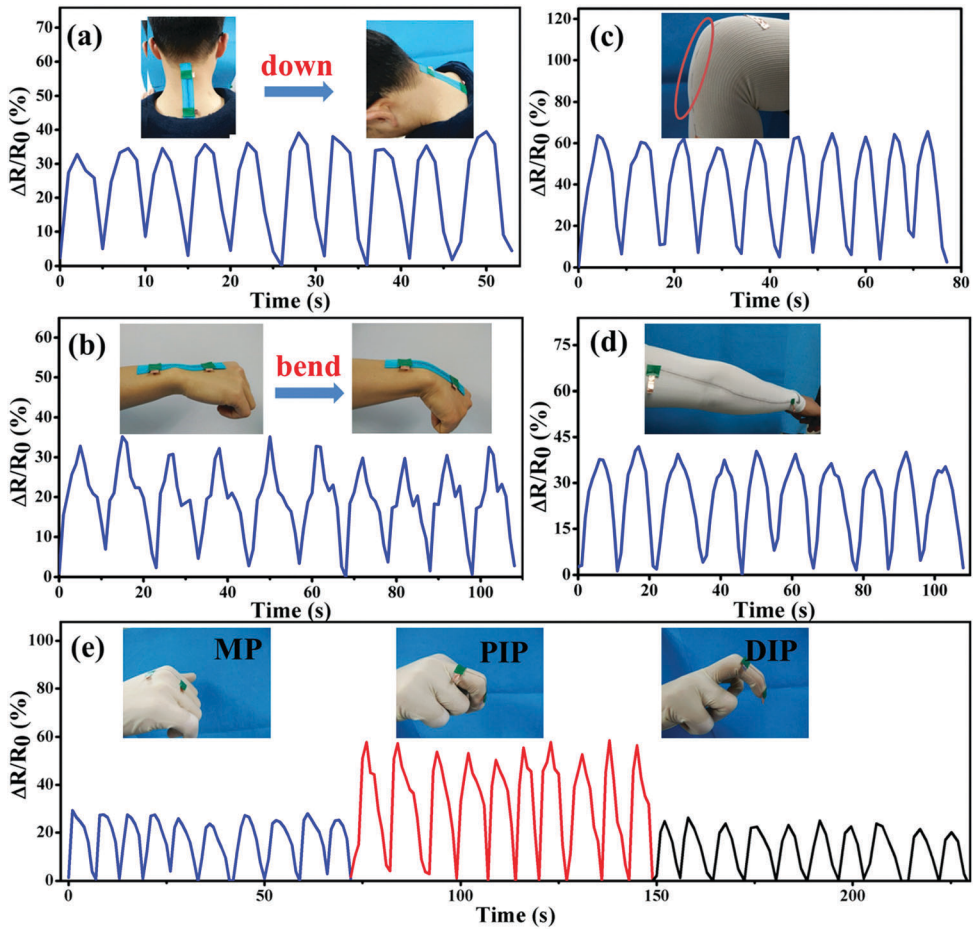

Fig. 9 The monitoring of human motion using the SMTY strain sensors. The response to the motions of neck bending (a), wrist bending (b), knee joint bending (c), elbow bending (d) and finger joint bending (e). The insets in each graph show the detailed photographs of the strain sensors.

As can be seen in Fig. 9e, the motions of different joints are easily recognized. Clearly, PIP has a large deformation during finger bending, which results in the largest signal peaks of the three tests. All the above results demonstrate the capability of the SMTY strain sensor in monitoring the large deformation of the human body.

4 Conclusions

A continuous electrospun SWNT/MWNT/TPU yarn (SMTY) with high conductivity and stretchability was successfully fabricated by a combined electrospinning, ultrasonication adsorbing, and bobbin winding process. The successive decoration of the MWNTs and SWNTs exhibited a synergistic effect to obtain higher conductivity, as well as the mechanical and thermal properties of the electrospun TPU fiber yarn. The conductive and stretchable SMTY also showed promising potential as wearable strain sensors. The fabricated SMTY strain sensor exhibited excellent stretchability (up to 100%) and stability (2000 cycles), and could be used to monitor large- and small-scale human body motions. Moreover, it can be knitted into textiles to fabricate large area electronic fabrics because of its fiber-shaped structure. In short, such a conductive and stretchable SMTY, fabricated by a low-cost and scalable method, exhibits promising potential in wearable electronics.

Conflicts of interest

There are no conflicts to declare.

Acknowledgements

We express our great thanks to the National Natural Science Foundation of China (11432003, 11572290) and the Major State Basic Research Projects (2012CB025904), HASTIT and Plan for Scientific Innovation Talent of the Henan Province, for the financial support.

References

1 W. Zeng, L. Shu, Q. Li, S. Chen, F. Wang and X. M. Tao, *Adv. Mater.*, 2014, **26**, 5310–5336.
2 Y. Tai and G. Lubineau, *Adv. Funct. Mater.*, 2016, **26**, 4037.
3 M. Stoppa and A. Chiolerio, *Sensors*, 2014, **14**, 11957–11992.

4 J. Ge, L. Sun, F. R. Zhang, Y. Zhang, L. A. Shi, H. Y. Zhao, H. W. Zhu, H. L. Jiang and S. H. Yu, *Adv. Mater.*, 2016, **28**, 722–728.
5 C. T. Huang, C. L. Shen, C. F. Tang and S. H. Chang, *Sens. Actuators, A*, 2008, **141**, 396–403.
6 X. Zhang, Z. Qin, X. Liu, B. Liang, N. Liu, Z. Zhou and M. Zhu, *J. Mater. Chem. A*, 2013, **1**, 10327–10333.
7 X. Liu, Z. Y. Qin, X. L. Zhang, L. Chen and M. F. Zhu, *Adv. Mater. Res.*, 2013, **750**, 55–58.
8 B. Karaguzel, C. R. Merritt, T. Kang, J. M. Wilson, H. T. Nagle, E. Grant and B. Pourdeyhimi, *J. Text. Inst.*, 2009, **100**, 1–9.
9 X. Wu, Y. Han, X. Zhang and C. Lu, *ACS Appl. Mater. Interfaces*, 2016, **8**, 9936–9945.
10 W. Weng, P. Chen, S. He, X. Sun and H. Peng, *Angew. Chem., Int. Ed.*, 2016, **55**, 6140.
11 (*a*) K. Liu, Y. Sun, R. Zhou, H. Zhu, J. Wang, L. Liu, S. Fan and K. Jiang, *Nanotechnology*, 2010, **21**, 045708; (*b*) M. Zhao, L. Meng, L. Ma, X. Yang, Y. Huang, J. Ryu, A. Shankar, T. Li, C. Yan and Z. Guo, *Compos. Sci. Technol.*, 2018, **154**, 28–36; (*c*) S. M. Aqeel, Z. Huang, J. Walton, C. Baker, D. Falkner, Z. Liu and Z. Wang, *Adv. Compos. Hybrid Mater.*, 2018, DOI: 10.1007/s42114-017-0002-5; (*d*) K. Zhang, G. Li, L. Feng, N. Wang, J. Guo, K. Sun, K. Yu, J. Zeng, T. Li, Z. Guo and M. Wang, *J. Mater. Chem. C*, 2017, **5**, 9359–9369; (*e*) C. Lin, L. Hu, C. Cheng, K. Sun, X. Guo, Q. Shao, J. Li, N. Wang and Z. Guo, *Electrochim. Acta*, 2018, **260**, 65–72; (*f*) K. Sun, P. Xie, Z. Wang, T. Su, Q. Shao, J. Ryu, X. Zhang, J. Guo, A. Shankar, J. Li, R. Fan, D. Cao and Z. Guo, *Polymer*, 2017, **125**, 50–57; (*g*) Z. Wu, S. Gao, L. Chen, D. Jiang, Q. Shao, B. Zhang, Z. Zhai, C. Wang, M. Zhao, Y. Ma, X. Zhang, L. Weng, M. Zhang and Z. Guo, *Macromol. Chem. Phys.*, 2017, DOI: 10.1002/macp.201700357.
12 Y. He, W. Chen, C. Gao, J. Zhou, X. Li and E. Xie, *Nanoscale*, 2013, **5**, 8799–8820.
13 (*a*) X. Zhao, B. Zheng, T. Huang and C. Gao, *Nanoscale*, 2015, **7**, 9399–9404; (*b*) X. Wang, X. Liu, H. Yuan, H. Liu, C. Liu, T. Li, C. Yan, X. Yan, C. Shen and Z. Guo, *Mater. Des.*, 2018, **139**, 372–379; (*c*) C. Wang, M. Zhao, J. Li, J. Yu, S. Sun, S. Ge, X. Guo, F. Xie, B. Jiang, E. Wujcik, Y. Huang, N. Wang and Z. Guo, *Polymer*, 2017, **131**, 263–271; (*d*) T. Liu, K. Yu, L. Gao, H. Chen, N. Wang, L. Hao, T. Li, H. He and Z. Guo, *J. Mater. Chem. A*, 2017, **5**, 17848–17855; (*e*) Y. Wang, B. Wang, J. Wang, Y. Ren, C. Xuan, C. Liu and C. Shen, *J. Hazard. Mater.*, 2018, **344**, 849–856; (*f*) J. Zhao, L. Wu, C. Zhan, Q. Shao, Z. Guo and L. Zhang, *Polymer*, 2017, **133**, 272–287.
14 R. H. Baughman, A. A. Zakhidov and W. A. de Heer, *Science*, 2002, **297**, 787–792.
15 (*a*) J. N. Coleman, U. Khan, W. J. Blau and Y. K. Gun'Ko, *Carbon*, 2006, **44**, 1624–1652; (*b*) G. Yu, Y. Lu, J. Guo, M. Patel, A. Bafana, X. Wang, B. Qiu, C. Jeffryes, S. Wei, Z. Guo and E. K. Wujcik, *Adv. Compos. Hybrid Mater.*, 2018, DOI: 10.1007/s42114-017-0004-3.
16 X. Zhang, Q. Li, T. Yi, Y. Li, J. Y. Coulter, L. Zheng, Y. Zhao, Q. Jia, D. E. Peterson and Y. Zhu, *Small*, 2007, **3**, 244–248.
17 X. H. Zhong, Y. L. Li, Y. K. Liu, X. H. Qiao, Y. Feng, J. Liang, J. Jin, L. Zhu, F. Hou and J. Y. Li, *Adv. Mater.*, 2010, **22**, 692–696.
18 L. K. Randeniya, A. Bendavid, P. J. Martin and C. D. Tran, *Small*, 2010, **6**, 1806–1811.
19 M. Zhang, K. R. Atkinson and R. H. Baughman, *Science*, 2004, **306**, 1358–1361.
20 Y. L. Li, I. A. Kinloch and A. H. Windle, *Science*, 2004, **304**, 276–278.
21 Z. Yang, X. Sun, X. Chen, Z. Yong, G. Xu, R. He, Z. An, Q. Li and H. Peng, *J. Mater. Chem.*, 2011, **21**, 13772–13775.
22 K. Liu, Y. Sun, X. Lin, R. Zhou, J. Wang, S. Fan and K. Jiang, *ACS Nano*, 2010, **4**, 5827–5834.
23 A. M. Beese, S. Sarkar, A. Nair, M. Naraghi, Z. An, A. Moravsky, R. O. Loutfy, M. J. Buehler, S. T. Nguyen and H. D. Espinosa, *ACS Nano*, 2013, **7**, 3434–3446.
24 J. Zhong, J. Meng, Z. Yang, P. Poulin and N. Koratkar, *Nano Energy*, 2015, **17**, 330–338.
25 M. Abbasipour and R. Khajavi, *Adv. Polym. Technol.*, 2013, **32**, 1158–1168.
26 R. Zhang, H. Deng, R. Valenca, J. Jin, Q. Fu, E. Bilotti and T. Peijs, *Sens. Actuators, A*, 2012, **179**, 83–91.
27 H. Qi, B. Schulz, T. Vad, J. Liu, E. Mäder, G. Seide and T. Gries, *ACS Appl. Mater. Interfaces*, 2015, **7**, 22404–22412.
28 N. M. Uddin, F. Ko, J. Xiong, B. Farouk and F. Capaldi, *Res. Lett. Mater. Sci.*, 2009, **2009**, 5–9.
29 X. Guan, G. Zheng, K. Dai, C. Liu, X. Yan, C. Shen and Z. Guo, *ACS Appl. Mater. Interfaces*, 2016, **8**, 14150–14159.
30 M. Ji, H. Deng, D. Yan, X. Li, L. Duan and Q. Fu, *Compos. Sci. Technol.*, 2014, **92**, 16–26.
31 K. Suzuki, K. Yataka, Y. Okumiya, S. Sakakibara, K. Sako, H. Mimura and Y. Inoue, *ACS Sens.*, 2016, **1**, 817–825.
32 L. Valentini, J. Biagiotti, J. M. Kenny and S. Santucci, *Compos. Sci. Technol.*, 2003, **63**, 1149–1153.
33 A. M. Bittner, M. Zhu, Y. Yang, H. F. Waibel, M. Konuma, U. Starke and C. J. Weber, *J. Power Sources*, 2012, **203**, 262–273.
34 T. Mcnally, P. Pötschke, P. Halley, M. Murphy, D. Martin, S. E. J. Bell, G. P. Brennan, D. Bein, P. Lemoine and J. P. Quinn, *Polymer*, 2005, **46**, 8222–8232.
35 J. Gao, M. Hu, Y. Dong and R. K. Y. Li, *ACS Appl. Mater. Interfaces*, 2013, **5**, 7758–7764.
36 H. Liu, M. Dong, W. Huang, J. Gao, K. Dai, J. Guo, G. Zheng, C. Liu, C. Shen and Z. Guo, *J. Mater. Chem. C*, 2017, **5**, 73–83.
37 H. Hu, L. Zhao, J. Liu, Y. Liu, J. Cheng, J. Luo, Y. Liang, Y. Tao, X. Wang and J. Zhao, *Polymer*, 2012, **53**, 3378–3385.
38 X. Li, H. Deng, Z. Li, H. Xiu, X. Qi, Q. Zhang, K. Wang, F. Chen and Q. Fu, *Composites, Part A*, 2015, **68**, 264–275.
39 A. K. Barick and D. K. Tripathy, *J. Mater. Sci. Eng. B*, 2011, **176**, 1435–1447.
40 J. Gao, M. Hu and R. K. Y. Li, *J. Mater. Chem.*, 2012, **22**, 10867–10872.
41 J. W. Zha, Y. Gao, D. L. Zhang, Y. Wen, R. K. Y. Li, C. Y. Shi and Z. M. Dang, *Compos. Sci. Technol.*, 2016, **128**, 201–206.
42 N. Wang, Z. Xu, P. Zhan, K. Dai, G. Zheng, C. Liu and C. Shen, *J. Mater. Chem. C*, 2017, **5**, 4408–4418.
43 Q. Fan, Z. Qin, S. Gao, Y. Wu, J. Pionteck, E. Mäder and M. Zhu, *Carbon*, 2012, **50**, 4085–4092.
44 Z. D. Huang, B. Zhang, S. W. Oh, Q. B. Zheng, X. Y. Lin, N. Yousefi and J. K. Kim, *J. Mater. Chem.*, 2012, **22**, 3591–3599.

45 L. Hu, M. Pasta, F. L. Mantia, L. Cui, S. Jeong, H. D. Deshazer, J. W. Choi, S. M. Han and Y. Cui, *Nano Lett.*, 2010, **10**, 708–714.
46 L. Liu, A. H. Barber, S. Nuriel and H. D. Wagner, *Adv. Funct. Mater.*, 2005, **15**, 975–980.
47 Z. Wang, Y. Huang, J. Sun, Y. Huang, H. Hu, R. Jiang, W. Gai, G. Li and C. Zhi, *ACS Appl. Mater. Interfaces*, 2016, **8**, 24837–24843.
48 Y. Zheng, Y. Li, Z. Li, Y. Wang, K. Dai, G. Zheng, C. Liu and C. Shen, *Compos. Sci. Technol.*, 2017, **139**, 64–73.
49 C. T. Huang, C. F. Tang, M. C. Lee and S. H. Chang, *Sens. Actuators, A*, 2008, **148**, 10–15.
50 M. Zhang, C. Wang, W. Qi, M. Jian and Y. Zhang, *ACS Appl. Mater. Interfaces*, 2016, **8**, 20894–20899.
51 Z. Wang, H. Yan, J. Sun, H. Yang, H. Hong, R. Jiang, W. Gai, G. Li and C. Zhi, *ACS Appl. Mater. Interfaces*, 2016, **8**, 24837–24843.